Electrochimica Acta 58 (2011) 699–706

Contents lists available at SciVerse ScienceDirect

Electrochimica Acta

journal homepage: www.elsevier.com/locate/electacta

Tunable electrochemical preparation of cobalt micro/nanostructures and their morphology-dependent wettability property

Ri Qiu[a,b], Dun Zhang[a,*], Peng Wang[a], Xiao Li Zhang[c], Young Soo Kang[d]

[a] Key Lab of Corrosion Science, Shandong Province, Institute of Oceanology, Chinese Academy of Sciences, 7 Nanhai Road, Qingdao 266071, China
[b] Graduate School of the Chinese Academy of Sciences, 19 (Jia) Yuquan Road, Beijing 100039, China
[c] ARC Centre of Excellence for Electromaterials Science, Monash University, Clayton 3800, Australia
[d] Department of Chemistry, Sogang University, Seoul 121-742, Republic of Korea

ARTICLE INFO

Article history:
Received 11 June 2011
Received in revised form 6 October 2011
Accepted 6 October 2011
Available online 15 October 2011

Keywords:
Electrochemical crystal growth
Cobalt morphology
Critical overpotential
Superhydrophobicity
Superhydrophilicity

ABSTRACT

A versatile cobalt micro/nanostructure preparation method via a facile electrochemical growth approach is reported in this study. Based on the existing theoretical analysis, the various crystal growth parameters, including the potential, concentration and temperature, act as parameters to impact the metallic crystal growth rate and the resultant morphology. These parameters were varied to elucidate the growth rate and morphology changes. Electron microscopy technique was applied to reveal the corresponding crystal morphology, which demonstrates that the potential can consequently impact the crystal shapes formed, from bump to flower and dendrite shapes. However, in the current experiments, the morphology achieved by changing the concentration and temperature was a dendritic structure, which suggests that the growth conditions promoted a dendritic structure formation regime. Based on the structures grown at various potentials, without further surface modifications, a morphology-dependent wettability trend exhibited from the superhydrophobic to superhydrophilic structures. The superhydrophobicity stems from the small contact areas of the tips of the flower-like structure. Meanwhile, the superhydrophilicity is due to the nanometer-scale channels existing in the hierarchical structures of the dendritic crystals, in which the capillary effect draws water droplets to spread on the surface rapidly.

1. Introduction

In the fields related to micro/nano-structured material, there is still widespread interest in developing solid substances with different external morphologies because the properties of the materials are critically determined by their external shapes [1]. Currently, attempts to prepare crystals with versatile morphologies continues at an intensified pace. Among the various shapes formed, fractal structures exhibiting aesthetic external shapes, such as flowers and dendrites, have attracted much attention due to their theoretical significance and potential applications [2a]. Particularly, the dendritic structures [2b], which are characterized as hierarchical configurations containing different ordered units, such as secondary, tertiary and even quaternary branches, have been constructed from a number of materials, including metal elements [3–8], alloys [9,10] and inorganic compounds [11–15]. Cobalt metal, which is one of the most important ferromagnetic materials, has been fabricated into numerous micro/nanometer scale materials with diverse morphologies via different approaches. Among them, hierarchical structures have been prepared previously by several groups [16–19], and their typical preparations have relied on hydrothermal/solvothermal methods, which require high temperatures and pressures during the preparation process. However, the preparation of cobalt materials using an electrochemical method, which is a standard approach to metallic material formation, has also been used in previous studies. For example, due to their underlying interest in fractal theory, Imre and his coworker applied an electrochemical technique to yield centimeter-scale cobalt dendrites [20,21]. Bodea et al. used electron microscopy to follow cobalt material growth under the influence of a magnetic field [22]. Based on these findings, a systematical electrochemical method study of different parameters that affect the growth of versatile metallic cobalt materials is worth being researched.

On the other hand, the extreme wettability phenomena, i.e., superhydrophobicity and superhydrophilicity, have drawn great attention in the material science and technology fields [23,24]. To date, various materials, such as metal oxide, silicon, carbon and metals, have been proven to illustrate the superhydrophobicity, superhydrophilicity, or dual function mutations with external impulsions. In 1944, Cassie and Baxter [25] demonstrated the well-known equation $\cos\theta_c = \Phi(\cos\theta_Y + 1) - 1$ to describe the wettability property of a rough surface. In this equation, θ_c is the

* Corresponding author. Tel.: +86 532 82898960; fax: +86 532 82898960.
E-mail address: zhangdun@qdio.ac.cn (D. Zhang).

0013-4686/$ – see front matter © 2011 Elsevier Ltd. All rights reserved.
doi:10.1016/j.electacta.2011.10.028

measured contact angle, θ_Y is the intrinsic contact angle to the water (known as the Young contact angle), and Φ is the surface fraction in contact with the liquid. This equation illustrates that the surface topology, composed of the micro/nanostructures of various shapes, makes critical contributions to its wettability. As θ_Y is a constant for the material utilized to modify the surface property, the relationship between cos θ_c and Φ is linear. When Φ adopts an extremely small value, θ_c will be large, and superhydrophobicity ($\theta_c > 150^\circ$) will occur, regardless of the intrinsic properties of the material [26]. Meanwhile, when Φ adopts a large value, a small θ_c will result, and the superhydrophilic ($\theta_c < 5^\circ$) phenomenon will appear. To the best of our knowledge, micro/nanostructure metallic cobalt structures exhibiting both superhydrophobicity and superhydrophilicity only originating from the morphology variations of the flower and dendrite-like shapes, has not been presented in previous study.

In this study, we present a metallic cobalt micro/nanostructure preparation via a simple electrochemical crystal growth route. Different parameters, including potential, concentration and temperature, were analyzed for their impacts on the crystal growth rate and the resultant morphology. Moreover, the as-prepared materials were found to show a range of wettabilities due to surface morphology differences. The flower-like structure exhibited superhydrophobicity without any modification of the hydrophobic organic molecules; in addition, the dendritic structure demonstrated intrinsic superhydrophilicity due to the capillary effect.

2. Experimental

2.1. Preparation and characterization of metallic cobalt structures

A typical electrolysis process for cobalt crystal growth was conducted as follows. All electrochemical experiments were performed on a CHI 760 electrochemical workstation. A simple three-electrode cell was used as the electrochemical reactor. The Cu foil (99.98% purity), which was scratched by abrasive paper and cleaned with deionized water (Millipore Filtration System), was used as the working electrode for cobalt crystal growth. The apparent surface area of the working electrode was *ca.* $2 \times 0.4\,cm^2$. A coiled Pt wire electrode acted as the counter electrode and a saturated calomel electrode (SCE) as the reference electrode. If there is no special indication, all potentials in this report are quoted with SCE. The distance between the working and counter electrodes was *ca.* 1.5 cm, and the tip of the reference electrode was placed near the edge of the working electrode. A 10 ml mixed solution containing $CoCl_2$ (Aldrich) and 0.1 M Na_2SO_4 (Shinyo Pure Chemicals, G.R. reagent) was for the electrolysis.

Different potentials (i.e., −0.8, −1.0 and −1.2 V) were applied for metallic cobalt crystal growth from the aforementioned mixed solution. The temperature was maintained in a water bath according to the experimental requirements. When the electrolysis process was completed, the electrode was brought from the aqueous solution and rinsed with Millipore water several times to remove impurities.

The external morphology of the as-grown material was revealed by different sophisticated techniques, including field-emission scanning electron microscopy (FE-SEM, JEOL, JSM-6700F) and high-resolution transmission electron microscope (HRTEM, JEOL. JEM-2010). Selected area electron diffraction (SAED, JEOL. JEM-2010, 200.0 KV) was adopted to reveal the fringe crystal structure of the as-obtained material. X-ray powder diffraction (XRD, PHILIPS, X'Pert-MPD System; X-ray was Cu Kα radiation with λ = 0.154056 nm) was utilized to verify the material crystal phase of the deposit scratched off from the copper substrate.

2.2. Wettability measurement

The wettability properties of the as-prepared material were measured with a contact angle meter (JC2000C1, Shanghai Zhongchen Digital Technique Apparatus Co., Ltd.) at ambient temperature. The water droplet used for the contact angle measurement was *ca.* 2 μL.

3. Results and discussion

3.1. Theoretical background of electrochemical crystal growth

Metal crystal growth driven by electrochemical motivation in a solution containing corresponding metal ions occurs according to the following equation

$$M^{n+}(aq) + ne^- = M(s) \quad (1)$$

During the electrolysis process, when the exerted potential is more negative than that of the equilibrium state between the ion and the metal, a net ion reduction reaction will occur on the electrode surface, and the ordered accumulation of metallic atoms will generate crystals. During the metal electrocrystallization process, the various external crystal morphologies, such as film, powder or fractal/dendrite shapes, will be produced, depending on the thermodynamics and kinetics conditions. The process of forming fractals or dendrites is more complex than the process that occurs when forming flat films on a substrate. The fractals and dendrites are formed as a result of the microscopically unsmooth surface and unstable hydrodynamics. The theoretical interpretation of these phenomena extends back to research performed in the 1960s [27]. Several theories, such as diffusion-limited aggregation [28], migration-limited mass-transfer [29] and the fractal propagation model [30], primarily describe the occurrence, propagation and resultant morphology of the complicated two-dimensional dendritic structure [31].

In this report, electrocrystallization was conducted in a three-dimensional geometry cell, and a supporting electrolyte was used for neglecting the electrical migration. Crystal growth on the electrode surface is considered to be controlled only by electrochemical activation and diffusion mass transfer. Barton and Bockris made a groundbreaking contribution to model this system, in which the fractal/dendritic structure can be formed only when the applied potential surpasses a critical value [27]. Following the pioneering work of Barton and Bockris, Popov et al. extended this model to the electrocrystallization of metal dendritic structures, such as Zn and Cu, based on theoretical and experimental results. It has been proposed that the process of fractal formation, and the formation of dendritic structures in particular, occurs in two steps: the initial state and the propagation process. In the initial state, an irregularity is formed on the electrode because of the unevenness of the substrate. Although the substrate appears to be smooth to the naked eye, microscopic protrusions inevitably exist. During the initial stage, the current density i_L normal to the surface plane is expressed according to the following equation:

$$i_L = \frac{nFDC_0}{\delta} \quad (2)$$

where D, C_0 and δ represent the diffusion coefficient, the bulk concentration of the ion and the diffusion layer thickness, respectively [27c]. Because these protrusions have a shorter distance (smaller δ) to the diffusion layer compared with the neighboring flat zones, a higher current density develops, and the protrusion will grow more rapidly than at the flat zone according to the following equation:

$$H_{i,t} = H_{i,0} \exp\left(\frac{t}{\tau}\right) \quad \tau = \frac{\delta^2 \rho}{MC_0 D} \quad (3)$$

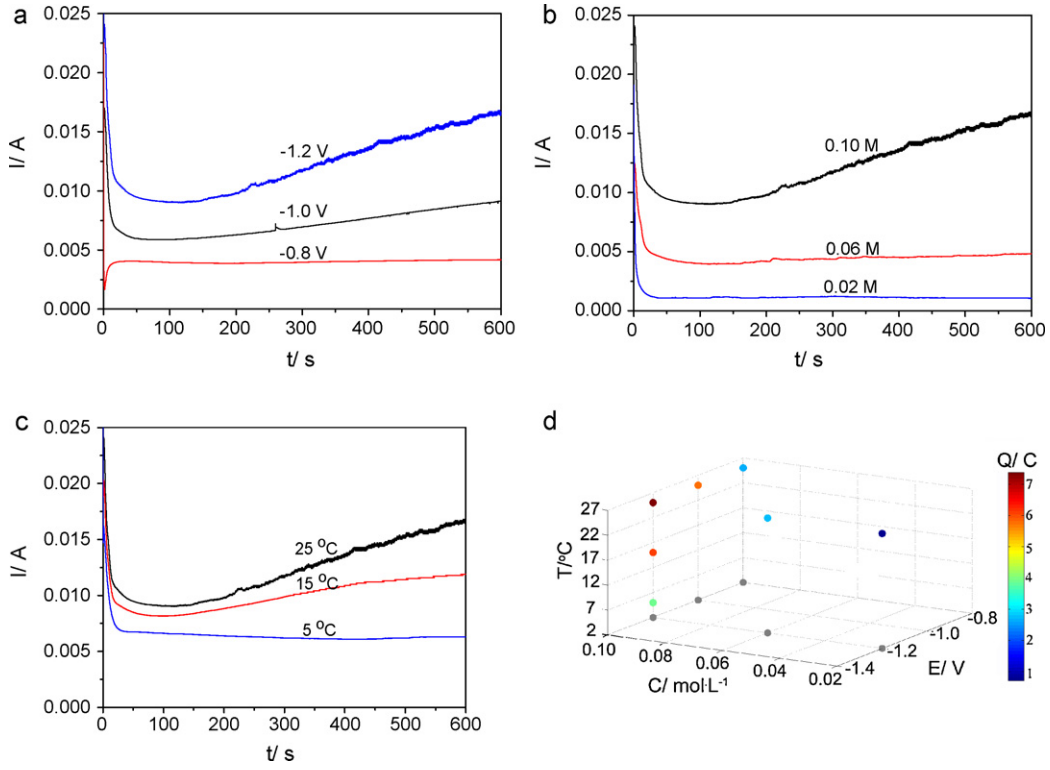

Fig. 1. *I–t* curves of different electrolysis conditions to electrochemically grow cobalt crystals. (a) 25 °C and 0.1 M $CoCl_2$ solution but different potentials; (b) 25 °C and −1.2 V but different $CoCl_2$ solutions; (c) 0.1 M $CoCl_2$ and −1.2 V but different temperatures; (d) the electron charge during the various electrochemical crystal growth processes.

In Eq. (3), M and ρ represent the molecular weight and density of the metal, respectively, and other parameters have their common connotations [32a]. Because of this non-homogeneous growth, the surface irregularity is amplified after the initial stage. The propagation process will form a dendritic structure only when the exerted overpotential exceeds a critical value. In this process, the irregularity developed in the initial stage will propagate into a tree-like appearance by which the "dendrite" is nominated. It has been shown in a previous report that dendrites can grow according to the following equation:

$$H_p = H_{p,0}\ \exp(k\eta^2 t) \tag{4}$$

in which $H_{p,0}$ is the as-grown height of the surface irregularity in the initial stage, and k is a constant [32b]. Based on Eq. (4), after the initial dendrite formation step, the as-grown length is exponentially related to the quadratic overpotential [32]. It is clear that when a larger overpotential is applied, the dendrites will have a faster growth rate.

The relationship between the bulk solution concentration C_0 and the reaction temperature T with dendrite growth was also studied by Popov and his colleagues [33,34]. They indicated that the minimum overpotential required for the initiation of dendrite growth depends on the precursor concentration according to the following equation:

$$\eta \approx \text{const.} + 60 \log C_0 \tag{5}$$

which means that a higher C_0 value requires a more negative potential to stimulate dendrite formation. However, during metal electrocrystallization under natural convection, i_L varies with the concentration as $i_L \approx kC_0^{1.25}$. At higher concentrations, the growth will be enhanced with a larger i_L, even when the overpotential for the initiation of dendrite growth acquires a larger value [33]. For the temperature to influence the dendrite formation and propagation, a previous study showed that an increase in temperature leads to the enhancement of the limiting diffusion current density, which produces additional feedstock for metal growth. Moreover, with increasing temperature, the overpotential required to initiate the dendrite growth decreases. Based on these two trends, high temperature favors the initiation and propagation of dendrites [34]. In this study, we will use the theoretical interpretation mentioned above to guide our practical experiments and to verify the impacts of various parameters (η, C and T) on the crystal growth rate and the final external morphology.

3.2. *The characterization of cobalt crystal growth based on the electrochemical method*

Based on the chronoamperometry technique, the relationship between the consumed electron rate I and the crystal growth time t can be measured *in situ* as the *I–t* curve during the electrochemical crystal growth process. In addition, the crystal growth rate is defined as $v = dL/dt$, in which L represents the propagation length, and t is the crystal growth time. Using the reaction described in Eq. (1) as an example, the grown crystal mass is expressed as $m = MQ/nF$, in which M is the atomic weight of the deposited metal, Q is the electron charge for crystal growth and F is the Faraday constant, and $m = \rho LS$, in which ρ and S are the metal density and as-grown dendrite area, respectively. Based on the equation $MQ/nF = \rho LS$, $L = MQ/\rho SnF$. When dendrite propagation occurs on the electrode, it is deduced that $v = dL/dt = d(MQ/\rho SnF)/dt = iV/nF$, in which i and V represent the current density and molar volume of the metal [27a], respectively. Because V, n and F are constants during the electrocrystallization process, if the deposited atoms do not migrate a significant distance away from the site where they are discharged, the crystal growth rate is proportional to the transient current density, which is determined using the *I–t* curve. Therefore, without considering the unit difference, the *I–t* curves shown in Fig. 1 represent the growth rate versus growth time when

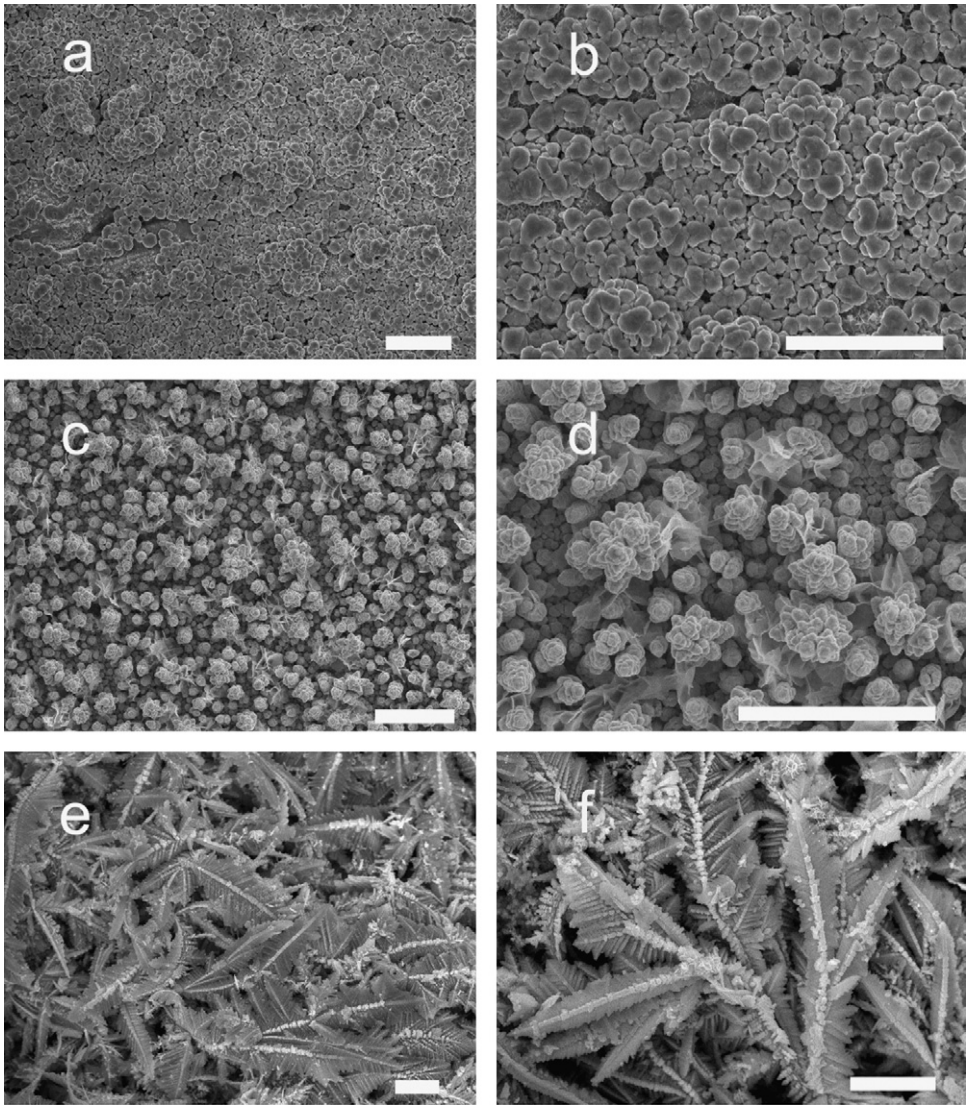

Fig. 2. FE-SEM images of Co material obtained at the same temperature (25 °C) and concentration (0.1 M $CoCl_2$) but different potentials of (a, b) – 0.8, (c, d) −1.0, (e, f) −1.2 V. All of the materials were obtained with an electrolysis time of 600 s. The temperature was maintained at 25 °C. All the bars in the figure represent 10 μm.

the side reactions are negligible (During our experiments, H_2 bubbling was not observed, which implies that the side reactions are negligible). As shown in Fig. 1(a–c), at the primary stage of crystal growth, incremental changes in the potential, temperature and concentration steadily enhanced the growth rate. A more negative potential, higher temperature and higher concentration can produce a stronger driving force during crystal growth. When the electrolysis time was greater than *ca.* 100 s, the current tended to increase during the crystal growth process, which is caused by the enlargement of the actual electrode surface, as demonstrated in previous investigations [8,9]. In the three-dimensional system of coordinates shown in Fig. 1(d), the colored points represent the electron charge consumed during the crystal growth process with three different parameters. The changing colors indicate that a larger driving force will result in a larger amount of metallic cobalt within the same time of crystal growth

Figs. 2–4 show the as-grown crystal morphology, depending on the different conditions. As shown in Fig. 2, the cobalt can exhibit a series of morphologies (i.e., bumps, flowers and dendrites) when subjected to variations in the applied crystal growth potential at the same precursor concentration and temperature. Fig. 2(a) and (b) shows that the crystals appear to be bump shaped when the potential is −0.8 V. The bumps are widely distributed on the surface of the electrode with a scale of approximately 1 μm. Clusters formed as an aggregation of bumps, which can be clearly identified in Fig. 2(a) and (b). Fig. 2(b) shows that the as-obtained bumps are homogeneous in large areas, with scales ranging from 1 μm to approximately 2 μm. Moreover, it can be observed that the bumps are interconnected. Compact films can readily form during the electrocrystallization process because cobalt metal is considered to have a small exchange current density [35,36]. Because no dendrites were formed on the substrate, it can be concluded that the applied potential of −0.8 V is more positive than the critical value for dendritic structure formation. When the electrolysis potential shifts slightly to reach −1.0 V, as shown in Fig. 2(c) and (d), a flower-like fractal structure distributed on the electrode surface is observed. As shown in Fig. 2(d), regardless of whether a single-flower or double-flower body was formed, the structure exhibited a six-petal shape, which is attributable to the inherent properties of cobalt metal. A more negative potential (i.e., −1.2 V) resulted in the formation of dendrites instead of bumps and flowers, which is illustrated in Fig. 2(e) and (f). As shown in Fig. 2(e), the entire length of a dendrite can reach several tens of microns, and the side branches can continue to grow as next-generation dendrites. In

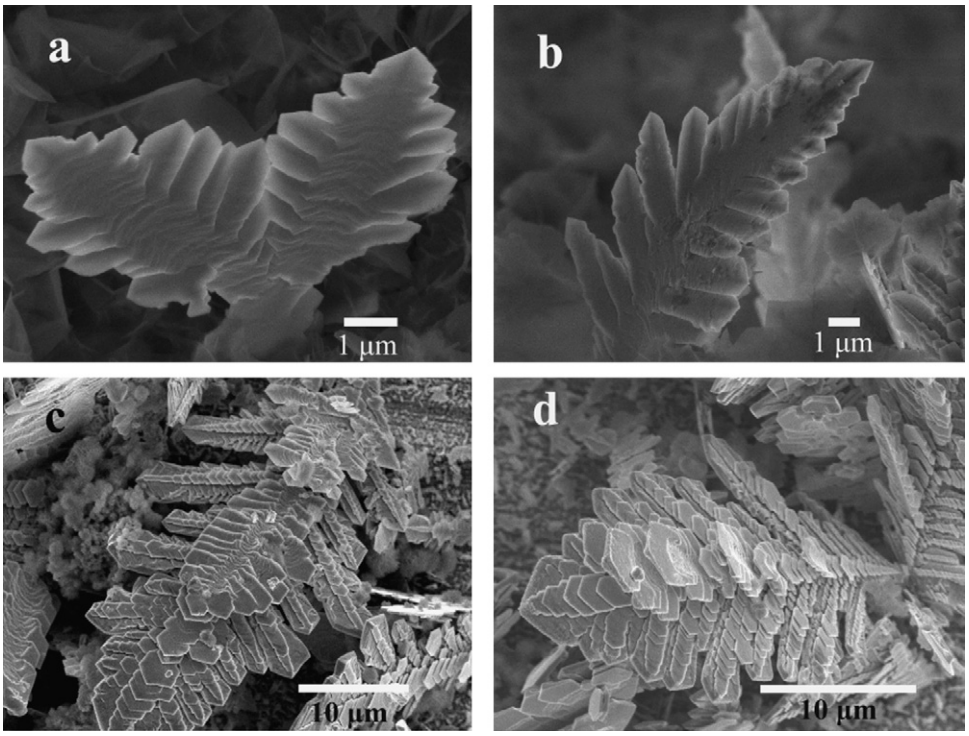

Fig. 3. Cobalt material morphology obtained at the same potential (−1.2 V) and temperature (25 °C) but different $CoCl_2$ concentration. (a, b) 0.02 M and (c, d) 0.06 M.

general, it is concluded that under the same solution concentration and electrolysis time, more negative potentials (i.e., a larger overpotential) will generate more complicated structures, such as flower- and dendrite-like fractal configurations. In the solution system containing 0.1 M $CoCl_2$ and 0.1 M Na_2SO_4 as the electrolytes, the critical potential for the fractal/dendritic initiation and propagation was found to be more negative than −0.8 V but more positive than −1.0 V.

Fig. 3 illustrates the concentration effect on the as-obtained material morphology. The figure shows that a low concentration but very negative potential of −1.2 V can also result in dendritic structures, although the scale will be smaller (*ca.* several microns) than for the more concentrated solution (*ca.* several tens of microns). This similarity in shape occurs because the applied potential plays a crucial role in the generation of dendritic structures, and the potential of −1.2 V exceeds the critical value. When

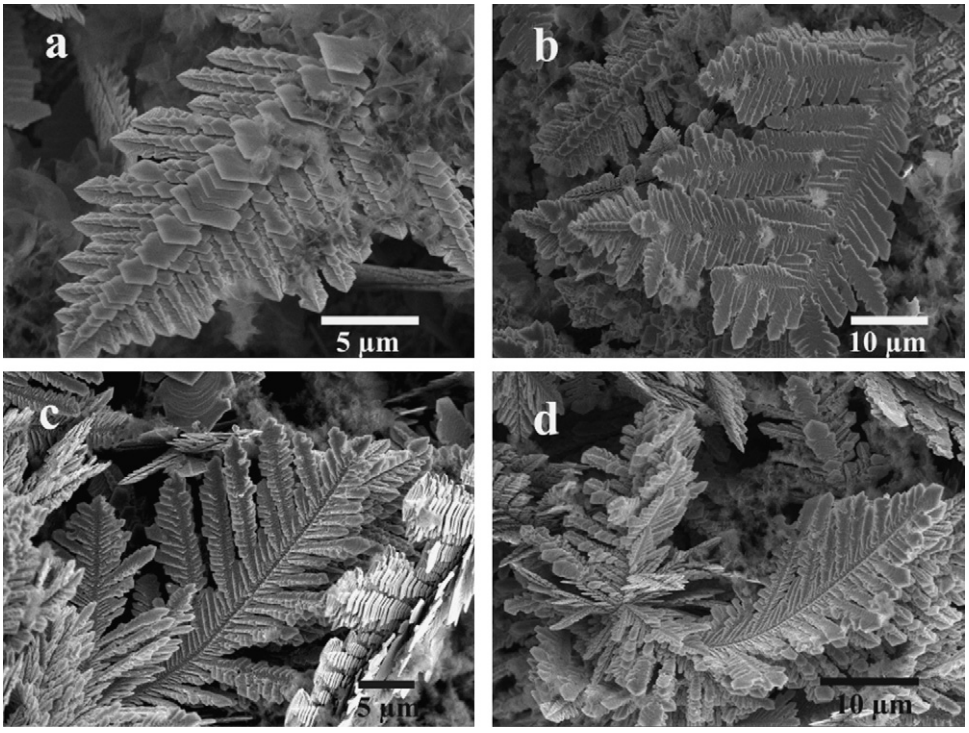

Fig. 4. Cobalt material morphology obtained at the same potential (−1.2 V) and $CoCl_2$ concentration (0.1 M) but different temperatures of (a, b) 5 °C and (c, d) 15 °C.

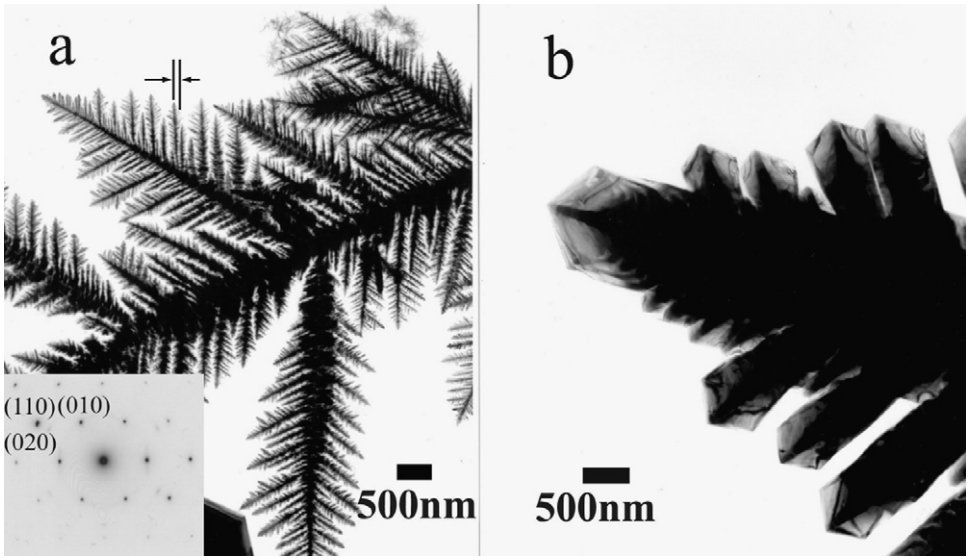

Fig. 5. HRTEM and SAED pattern of the deposit obtained at the potential −1.2 V.

comparing the *I*–*t* curve for −0.8 V in Fig. 1(a) and the 0.02 M curve in Fig. 1(b), it is found that after 25 s, the growth rate for −0.8 V is faster than with 0.02 M. However, crystal growth at −0.8 V only resulted in bumps, whereas growth at 0.02 M resulted in dendrites. According to the theory stated above, because the potential of −0.8 V is more positive than the critical potential, the irregularity in the substrate cannot complete the two stages to produce a fractal/dendritic morphology. As shown in Fig. 1(a), crystal growth under the potential of −0.8 V affords a slow growth rate during the initial 25 s, and the current is less than 4 mA. For crystal growth with a potential of −1.2 V and a concentration of 0.02 M, the rate is higher because of the strong current. This initial stage is critical for the subsequent electrocrystallization. During the initial stage, the protrusions on the surface are elongated, and these elongated protrusions form the basis for dendritic structure formation. Although the following current is lower than that of the system with a potential of −0.8 V, the primary step has already determined the impending dendritic characteristics. However, even though the growth rate is faster for a system with a potential of −0.8 V, the accumulated metal atoms thicken the bump film, and a dendritic structure will not be formed.

Fig. 4 illustrates the cobalt material morphology obtained at the same potential (−1.2 V) and $CoCl_2$ concentration (0.1 M) but at different temperatures. Because −1.2 V surpasses the critical potential for dendritic structure formation, there is no distinct difference in the external morphology shown with the two conditions, and the morphologies both exhibit hierarchical structure. However, the scale of the dendrites is different; the lower temperature led to the formation of shorter dendrites than with the higher temperature, which is attributable to the growth rate as discussed above. Based on Fig. 1(c), it is assumed that a higher temperature will increase the mass transfer rate during the crystal growth process such that the enhanced growth rate and a larger-scale crystal will eventually be realized during the same growth time.

Based on these theoretical and experimental results, it is concluded that the exerted potential plays a key role in determining the external morphology during the metal electrocrystallization process. Although the precursor concentration or reaction temperature may be decreased, if the applied potential exceeds the critical value, the dendritic structure can nevertheless be realized. The concentration and temperature can exert a force for driving the growth rate, which can change the scale of the achieved structure.

To further investigate dendrite formation, the HRTEM technique is used to reveal its precise structure. The images shown in Fig. 5 present two morphologies of the as-prepared cobalt dendrites. In Fig. 5(a), the hierarchical characteristics of the dendrite are clearly demonstrated. An individual cobalt dendrite structure is composed of a long central stem and secondary, tertiary, and even quaternary branches. The stem and all of the branches of different orders form the hierarchical structure. The different-ordered structures are similar, although the scale is dramatically dissimilar. From the main stem to the quaternary branches, the scale ranges from *ca.* 50 nm to several microns. Fig. 5(b) shows the flake-like form, in which the hexagonal crystal shape can be observed at the tips of the dendrite. Although there is a morphological difference between the two types of dendrites, the intrinsic features are the same. It is clear that the angles between the stems and branches are *ca.* 60°. The tips are less thick than the stems, so that the electron beams can penetrate the tips and obtain an electron diffraction pattern. As shown in the inset in Fig. 5(a), the SAED pattern of an as-obtained

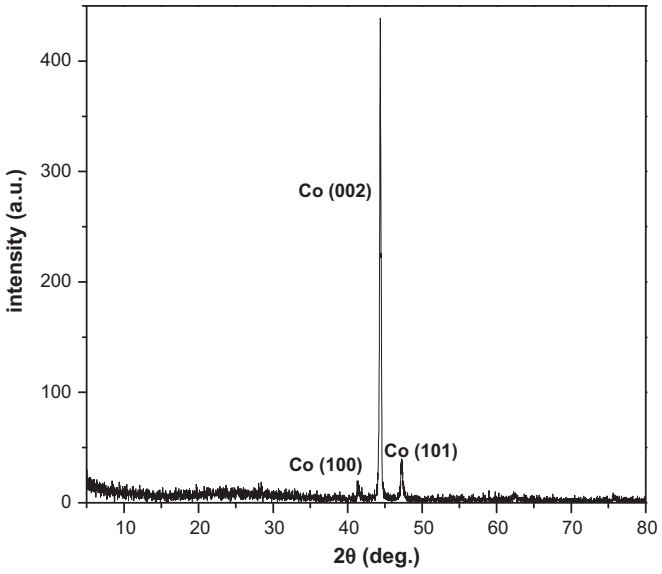

Fig. 6. XRD pattern of the deposit obtained at the potential −1.2 V and electrolysis time 1200 s from 0.1 M $CoCl_2$ at room temperature.

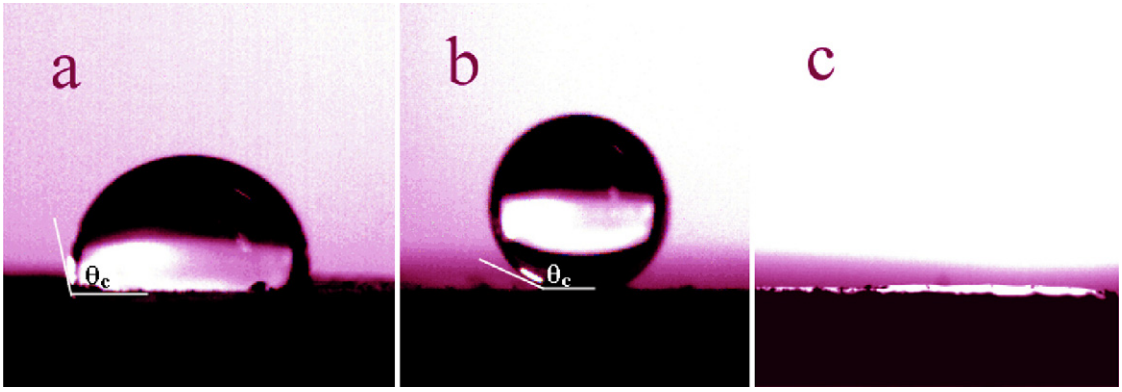

Fig. 7. Shape-dependent wettability property of metallic cobalt achieved with the same concentration (0.1 M $CoCl_2$), temperature (25 °C) and crystal growth time (600 s) but different imposed potentials of (a) −0.8 V, (b) −1.0 V and (c) −1.2 V.

dendrite indicates that the edge of the dendrite belongs to a single crystalline structure, and the as-achieved cobalt material is of a hexagonal phase.

The XRD pattern of the as-deposited dendrites is shown in Fig. 6. The three main diffraction peaks are indexed as the (1 0 0), (0 0 2) and (1 0 1) planes of the hexagonal cobalt crystal structure, which is recorded as JCPDS No. 89-7373.

3.3. Wettability of the surface modified by different cobalt morphologies

The contact angle test was used to evaluate the wettability properties of the materials prepared under various potentials. The wettability demonstrated a dramatic variation from hydrophilic, superhydrophobic to superhydrophilic behaviors that depend on the external morphology and coverage. As shown in Fig. 7(a) and (b), the contact angles are $102 \pm 2^\circ$ and $161 \pm 2^\circ$; however, the contact angle in (c) is less than 5°, which is characteristic of superhydrophilicity. The morphology plays a critical role in determining the surface wettability. For the bump-like structure, which shows hydrophilic wettability, the surface is relatively flat and smooth, and little air remained under the water droplets. This wettability property of the bump-like structure was similar to that of the bulk cobalt metal. However, the discrete flower-like structure grown on the substrate formed an upright matrix, which allows only the flower tips to contact the water droplet, with air remaining in the spaces. The contact area is relatively small so that a superhydrophobic behavior was exhibited [37]. In contrast, the dendritic structure showed the other extreme of wettability. As illustrated in Fig. 2(e) and (f), the dendrites were randomly distributed on the substrate, unlike the discrete flower structures standing on the substrate. Moreover, the vein structure of the dendrites plays a significant role in the observed superhydrophilicity. As indicated in Fig. 5(a), a vein structure can form channels among the neighboring branches in this hierarchical structure. A neighboring channel with a diameter of *ca.* 100 nm is highlighted. According to the Young–Laplace equation, $p = 2\gamma/R$, in which p is the additional pressure, and γ and R represent the water surface tension and radius of curvature, respectively. The capillary force p is approximated as $p = 2 \times 0.07214/(50 \times 10^{-9}) = 2.89 \times 10^6$ Pa. Under such a large force, the water droplet will spread rapidly along the dendrite veins, which leads to superhydrophilic wettability.

4. Conclusions

Cobalt micro/nanostructures with different external morphologies were prepared by the electrochemical growth method. It was demonstrated, based on both theoretical and practical perspectives, that various crystal growth parameters determine the metallic crystal growth rate and resultant morphology. Based on the structures achieved at various potentials, wettability, which ranges from superhydrophobic to superhydrophilic, depends on the morphology.

Acknowledgments

This work was supported by the National Natural Science Foundation of China (Grant No. 51131008 and No. 41076047) and the Chinese Academy of Sciences (Grant KZCX2-YW-205-03). Special appreciation is given to the Brain Korea 21 (BK 21) project.

References

[1] (a) A.D. Dinsmore, M.F. Hsu, M.G. Nikolaides, M. Marquez, A.R. Bausch, D.A. Weitz, Colloidosomes: selectively permeable capsules composed of colloidal particles, Science 298 (2002) 1006;
(b) X.S. Fang, C.H. Ye, L.D. Zhang, T. Xie, Twinning-mediated growth of Al_2O_3 nanobelts and their enhanced dielectric responses, Adv. Mater. 17 (2005) 1661;
(c) D. Seo, C.I. Yoo, J. Jung, H. Song, Ag–Au–Ag heterometallic nanorods formed through directed anisotropic growth, J. Am. Chem. Soc. 130 (2008) 2940;
(d) W. Ni, H. Chen, J. Su, Z. Sun, J. Wang, H. Wu, Effects of dyes, gold nanocrystals, pH, and metal ions on plasmonic and molecular resonance coupling, J. Am. Chem. Soc. 132 (2010) 4806.
[2] (a) B.B. Mandelbrot, The Fractal Geometry of Nature, W.H. Freeman, New York, 1983;
(b) P.K. Galenko, V.A. Zhuravlev, Physics of Dendrites: Computational Experiments, World Scientific, Singapore, 1994.
[3] X.M. Liu, S.Y. Fu, High-yield synthesis of dendritic Ni nanostructures by hydrothermal reduction, J. Cryst. Growth 306 (2007) 428.
[4] X.P. Sun, M. Hagner, Novel preparation of snowflake-like dendritic nanostructures of Ag or Au at room temperature via a wet-chemical route, Langmuir 23 (2007) 9147.
[5] G.D. Wei, C.W. Nan, Y. Deng, Y.H. Lin, Self-organized synthesis of silver chain-like and dendritic nanostructures via a solvothermal method, Chem. Mater. 15 (2003) 4436.
[6] L.H. Lu, A. Kobayashi, Y. Kikkawa, K. Tawa, Y. Ozaki, Oriented attachment-based assembly of dendritic silver nanostructures at room temperature, J. Phys. Chem. B 110 (2006) 23234.
[7] J.P. Xiao, Y. Xie, R. Tang, M. Chen, X.B. Tian, Novel ultrasonically assisted templated synthesis of palladium and silver dendritic nanostructures, Adv. Mater. 13 (2001) 1887.
[8] R. Qiu, H.G. Cha, H.B. Noh, Y.B. Shim, X.L. Zhang, R. Qiao, D. Zhang, Y.I. Kim, U. Pal, Y.S. Kang, Preparation of dendritic copper nanostructures and their characterization for electroreduction, J. Phys. Chem. C 113 (2009) 15891.
[9] R. Qiu, X.L. Zhang, R. Qiao, Y. Li, Y.I. Kim, Y.S. Kang, CuNi dendritic material: synthesis, mechanism discussion, and application as glucose sensor, Chem. Mater. 19 (2007) 4174.
[10] X.M. Zhou, X.W. Wei, Single crystalline $FeNi_3$ dendrites: large scale synthesis, formation mechanism, and magnetic properties, Cryst. Growth Des. 9 (2009) 7.
[11] M.H. Cao, T.F. Liu, S. Gao, G.B. Sun, X.L. Wu, C.W. Hu, Z.L. Wang, Single-crystal dendritic micro-pines of magnetic α-Fe_2O_3: large-scale synthesis, formation mechanism, and properties, Angew. Chem. Int. Ed. 44 (2005) 4197.
[12] W.P. Lim, H.Y. Low, W.S. Chin, From winter snowflakes to spring blossoms: manipulating the growth of copper sulfide dendrites, Cryst. Growth Des. 7 (2007) 2429.

[13] Y. Cheng, Y.S. Wang, D.Q. Chen, F. Bao, Evolution of single crystalline dendrites from nanoparticles through oriented attachment, J. Phys. Chem. B 109 (2005) 794.
[14] Z.R. Tian, J. Liu, J.A. Voigt, H.F. Xu, M.J. Mcdermott, Dendritic growth of cubically ordered manoporous materials through self-assembly, Nano Lett. 3 (2003) 89.
[15] D.B. Kuang, A.W. Xu, Y.P. Fang, H.Q. Liu, C. Frommen, D. Fenske, Surfactant-assisted growth of novel PbS dendritic nanostructures via facile hydrothermal process, Adv. Mater. 15 (2003) 1747.
[16] Y.C. Zhu, H.G. Zheng, Q. Yang, A.L. Pan, Z.P. Yang, Y.T. Qian, Growth of dendritic cobalt nanocrystals at room temperature, J. Cryst. Growth 260 (2004) 427.
[17] X.H. Liu, R. Yi, Y.T. Wang, G.Z. Qin, N. Zhang, X.G. Li, Highly ordered snowflake like metallic cobalt microcrystals, J. Phys. Chem. C 111 (2007) 163.
[18] (a) L.P. Zhu, H.M. Xiao, W.D. Zhang, Y. Yang, S.Y. Fu, Synthesis and characterization of novel three-dimensional metallic Co dendritic superstructures by a simple hydrothermal reduction route, Cryst. Growth Des. 8 (2008) 1113;
(b) X.M. Liu, W.L. Gao, S.B. Miao, B.M. Ji, Versatile fabrication of dendritic cobalt microstructures using CTAB in high alkali media, J. Phys. Chem. Solids 69 (2008) 2665.
[19] C.L. Jiang, L.Y. Wang, K. Kuwabara, Selective-precursor reducing route to cobalt nanocrystals and ferromagnetic property, J. Solid State Chem. 180 (2007) 3146.
[20] A.R. Imre, L. Balázs, Fractal behavior of tree-like nickel and cobalt electrodeposits, Fractals 8 (2000) 349.
[21] A. Imre, Z. Vértesy, T. Pajkossy, L. Nyikos, Morphology of cobalt electrodeposits, Fractals 1 (1993) 59.
[22] S. Bodea, R. Ballou, L. Pontonnier, P. Molho, Electrochemical growth of iron and cobalt arborescences under a magnetic field: a TEM study, Phys. Rev. B 66 (2002), 224104-1-6.
[23] (a) H.Y. Erbil, A.L. Demirel, Y. Acvi, O. Mert, Transformation of a simple plastic into a superhydrophobic surface, Science 299 (2003) 1377;
(b) F. Xia, L. Feng, S. Wang, T. Sun, W. Song, W. Jiang, L. Jiang, Dual-responsive surfaces that switch between superhydrophilicity and superhydrophobicity, Adv. Mater. 18 (2006) 432;
(c) Y. Li, C.C. Li, S.O. Cho, G.T. Duan, W.P. Cai, Silver hierarchical bowl-like array: synthesis, superhydrophobicity, and optical properties, Langmuir 23 (2007) 9802;
(d) Y. Li, T. Sasaki, Y. Shimizu, N. Koshizaki, Hexagonal-close-packed, hierarchical amorphous TiO_2 nanocolumn arrays: transferability, enhanced photocatalytic activity and superamphiphilicity without UV irradiation, J. Am. Chem. Soc. 130 (2008) 14755;
(e) L. Wang, X. Zhang, Y. Fu, B. Li, Y. Liu, Bioinspired preparation of ultrathin SiO_2 shell on ZnO nanowire array for ultraviolet-durable superhydrophobicity, Langmuir 25 (2009) 13619;
(f) J.C. Tuberquia, N. Nizamidin, R.R. Harl, J. Albert, J. Hunter, B.R. Rogers, G.K. Jennings, Surface-initiated polymerization of superhydrophobic polymethylene, J. Am. Chem. Soc. 132 (2010) 5725.
[24] (a) R. Wang, K. Hashimoto, A. Fujishima, M. Chikuni, E. Kijima, A. Kitamura, M. Shimohigoshi, T. Watanabe, Light-induced amphiphilic surfaces, Nature 388 (1997) 431;
(b) X. Yu, Z. Wang, Y. Jiang, X. Zhang, Surface gradient material: from superhydrophobicity to superhydrophilicity, Langmuir 22 (2006) 4483;
(c) W. Hou, Q. Wang, UV-driven reversible switching of a polystyrene/titania nanocomposite coating between superhydrophobicity and superhydrophilicity, Langmuir 25 (2009) 6875;
(d) J. Yang, Z. Zhang, X. Men, X. Xu, X. Zhu, Reversible superhydrophobicity to superhydrophilicity switching of a carbon nanotube film via alternation of UV irradiation and dark storage, Langmuir 26 (2010) 10198;
(e) L. Wang, B. Peng, Z. Su, Tunable wettability and rewritable wettability gradient from superhydrophilicity to superhydrophobicity, Langmuir 26 (2010) 12203.
[25] A.B.D. Cassie, S. Baxter, Wettability of porous surfaces, Trans. Faraday Soc. 40 (1944) 546.
[26] (a) E. Hosono, S. Fujihara, I. Honma, H. Zhou, Superhydrophobic perpendicular nanopin film by the bottom-up process, J. Am. Chem. Soc. 127 (2005) 13458;
(b) L. Cao, H.H. Hu, D. Gao, Design and fabrication of micro-textures for inducing a superhydrophobic behavior on hydrophilic materials, Langmuir 23 (2007) 4310;
(c) M. Karlsson, P. Forsberg, F. Nikolajeff, From hydrophilic to superhydrophobic: fabrication of micrometer-sized nail-head-shaped pillars in diamond, Langmuir 26 (2010) 889;
(d) Y. Li, X.J. Huang, S.H. Heo, C.C. Li, Y.K. Choi, W.P. Cai, S.O. Cho, Superhydrophobic bionic surfaces with hierarchical microsphere/SWCNT composite arrays, Langmuir 23 (2007) 2169;
(e) W. Xi, Z. Qiao, C. Zhu, A. Jia, M. Li, The preparation of lotus-like superhydrophobic copper surfaces by electroplating, Appl. Surf. Sci. 255 (2009) 4836.
[27] (a) J.L. Barton, J.O'M. Bockris, Proc. R. Soc. Lond. A 268 (1962) 485;
(b) J.W. Diggle, A.R. Despic, J.O'M. Bockris, J. Electrochem. Soc. 116 (1969) 1503;
(c) K.I. Popov, S.S. Djokić, B.N. Grgur, Fundamental Aspects of Electrometallurgy, Kluwer Academic Publishers, New York, 2002.
[28] T.A. Witten Jr., L.M. Sander, Diffusion-limited aggregation, a kinetic critical phenomenon, Phys. Rev. Lett. 47 (1981) 1400.
[29] (a) J.N. Chazalviel, Electrochemical aspects of the generation of ramified metallic deposits, Phys. Rev. A 42 (1990) 7355;
(b) V. Fleury, Branched fractal patterns in non-equilibrium electrochemical deposition from oscillatory nucleation and growth, Nature 390 (1997) 145.
[30] C. Chen, J. Jorne, Fractal analysis of zinc electrodeposition, J. Electrochem. Soc. 137 (1990) 2047.
[31] C. Monroe, J. Newman, The effect of interfacial deformation on electrodeposition kinetics, J. Electrochem. Soc. 151 (2004) A880.
[32] (a) K.I. Popov, Lj.M. Djukić, M.G. Pavlović, M.D. Maksimović, The critical overpotential for copper dendrite formation, J. Appl. Electrochem. 9 (1979) 527;
(b) K.I. Popov, M.G. Pavlović, M.D. Spasojević, V.M. Nakić, The critical overpotential for zinc dendrite formation J, Appl. Electrochem. 9 (1979) 533.
[33] N.D. Nikolić, K.I. Popov, L.J. Pavlović, M.G. Pavlović, Determination of critical conditions for the formation of electrodeposited copper structures suitable for electrodes in electrochemical devices, Sensors 7 (2007) 1.
[34] N.D. Nikolić, L.J. Pavlović, M.G. Pavlović, K.I. Popov, Effect of temperature on the electrodeposition of disperse copper deposits, J. Serb. Chem. Soc. 72 (2007) 1369.
[35] R. Winand, Electrodeposition of metals and alloys-new results and perspectives, Electrochim. Acta 39 (1994) 1091.
[36] K.I. Popov, M.G. Pavlovic, B.N. Grgur, A.T. Dimitrov, S.H. Jordanov, Electrodeposition of silver from nitrate solution: Part II. Mechanism of the effect of phosphate ions, J. Appl. Electrochem. 28 (1998) 797.
[37] R. Qiu, P. Wang, D. Zhang, J.J. Wu, One-step preparation of hierarchical cobalt structure with inborn superhydrophobic effect, Colloids Surf. A 377 (2011) 144.